Shock wave acceleration of protons in inhomogeneous plasma interacting with ultrashort intense laser pulses

Zs. Lecz[1] and A. Andreev[1,2]
[1]ELI-ALPS, Szeged, Hungary
[2]Max-Born Institute, Berlin, Germany

(Received 9 October 2014; accepted 10 February 2015; published online 3 April 2015)

The acceleration of protons, triggered by solitary waves in expanded solid targets is investigated using particle-in-cell simulations. The near-critical density plasma is irradiated by ultrashort high power laser pulses, which generate the solitary wave. The transformation of this soliton into a shock wave during propagation in plasma with exponentially decreasing density profile is described analytically, which allows to obtain a scaling law for the proton energy. The high quality proton bunch with small energy spread is produced by reflection from the shock-front. According to the 2D simulations, the mechanism is stable only if the laser pulse duration is shorter than the characteristic development time of the parasitic Weibel instability. © *2015 AIP Publishing LLC*.
[http://dx.doi.org/10.1063/1.4913438]

I. INTRODUCTION

Ion acceleration using ultrashort laser pulses with relativistic intensities has been investigated theoretically and experimentally during the last decade with the possible applications of high quality ion beams being the main driving force of this research. The high current, short duration, and ultra-low transversal emittance[1] make the resultant ion beams unique in accelerator physics and open up new methodology and applications in experimental diagnostics.[2,3] The very small transversal beam size combined with tight focusing abilities enables their employment in medical treatments[4] including cancer therapy.[5]

Several acceleration regimes have been identified and some have also been experimentally realized.[6] These regimes depend on the laser and target parameters. The most understood and well established mechanism is the target normal sheath acceleration (TNSA),[7,8] which is the consequence of strong charge separation induced by the laser-generated energetic electrons in solid targets. Due to the large charge to mass ratio, mostly protons are accelerated from the target surface. The thickness of an ever-present hydrogen-rich contamination layer affects the resultant proton beam spectral shape and thus potential applications. For very thin layers (∼nanometers), the protons are quasi-monoenergetic with low energy conversion efficiency and peak energy up to several MeV.[9,10] An exponential energy spectrum[11,12] is observed with higher energy conversion (up to 10%) and cut-off energy up to 50–70 MeV when a thick layer is present.

Increasing the intensity of the laser pulse results in the radiation pressure acceleration (RPA)[13,14] becoming a more dominant process occurring on the front side of the target. This mechanism provides higher energy conversion and a smaller energy spread at the same time than TNSA. These effects are particularly predominate for circularly polarized laser pulses, which ensures non-oscillating ponderomotive force.[15] The most efficient acceleration can be achieved in the laser-piston regime,[16] which requires ultra-thin solid targets; high peak intensity and very high contrast ratio of the main pulse. A more accessible regime is the shock wave acceleration (SWA),[17,18] which appears to be more efficient in near-critical density plasma. A significant number of protons have been observed within a narrow energy range in both simulations[19,20] and experiments.[21,22] In preceding experiments, gas targets and long-wavelength lasers were predominately used in order to ensure near-critical density laser-plasma interactions.

For high power lasers, the typical wavelength is much shorter, thus the critical density is higher, but still below the solid density. The SWA with solid foil targets can be realized by using a longer and much lower intensity preparatory pulse. The main pulse then interacts with an expanded, low density plasma.[23] In simulations, such targets can be modeled with a triangular density profile,[19,24] which is a reasonable approximation for long density scale lengths. However, the exact shape is not trivial and can be realistically reproduced by using hydro codes.[23,25] In this paper, the linear and exponential profiles are considered and the crucial differences between the two cases are discussed. Due to the short density scale-lengths and better beam quality observed after acceleration, this work focuses on the exponential density profile at the rear side of the plasma, which was also considered in Ref. 20. This density distribution naturally follows from the isothermal plasma expansion model,[11,26] which is probably the main process responsible for the plasma formation.

The choice of laser pulse parameters is inspired by the future ELI-ALPS facility, which will be the host of many short-pulse-related experiments. The planned laser beam energy is 15 J, compressed to about 20 fs duration, in the first phase of ELI-ALPS. Depending on the focusing, which will provide a 6–10 μm laser spot diameter, the dimensionless laser amplitude can be $a_0 \approx 20$–40, where $a_0^2 = I_L[10^{18}\mathrm{W/cm^2}]\lambda_L^2[\mu\mathrm{m}^2]/1.37$ and λ_L, I_L are the laser wavelength and intensity, respectively. The advantage of short pulse duration is the generation of a single strong shock wave, whereas with long pulses multiple peaks

 © 2015 AIP Publishing LLC

This article is copyrighted as indicated in the article. Reuse of AIP content is subject to the terms at: http://scitation.aip.org/termsconditions. Downloaded to IP: 129.81.226.78 On: Mon, 18 May 2015 08:13:37

appear in the velocity phase-space,[17,19] which results in a broader energy spread and less controllable acceleration. Even with a single shock wave in uniform plasma, the energy spectrum of accelerated protons will broaden after the interaction on a longer timescale.[17] For the realization of a stable and predictable acceleration mechanism, the combined effects of shock propagation and reduced rear side acceleration[27] in a decreasing density profile are exploited. A similar mechanism was presented in Ref. 20, but on a much longer time scale (~ps) and with much longer plasma scale lengths (>10 μm).

II. 1D PARTICLE-IN-CELL SIMULATIONS

The critical density can be expressed as $n_{cr} = 1/\lambda_L^2$ $[\mu m^2]10^{21}\,cm^{-3}$ or $n_{cr}^r = a_0 n_{cr}/\sqrt{2}$ with relativistic corrections, for linearly polarized laser light. In a gas target, 10 μm wavelength is necessary to obtain the SWA conditions for moderate laser intensity, which is possible with CO_2 lasers. The density of a solid target has to be decreased in order to realize the same acceleration mechanism with shorter wavelength lasers. For $a_0 \approx 20$ and $\lambda_L \approx 1$ μm, the critical density is $n_{cr}^r = 1.4 \times 10^{22}\,cm^{-3}$, which is only several times smaller than the density of solid hydrogen $n_0 \approx 6 \times 10^{22}\,cm^{-3}$.

A non-uniform plasma, which in the first approximation can be modeled with linear density profile, can be formed by firing a long, low-intensity pulse upon the target. In this simple geometry, the peak density can be written as $n_p = n_0/f$, where $f = 2C_{sc}t_e/d$, d and n_0 are the original thickness and density of the foil and $C_{sc} = \sqrt{T_c/m_p}$ is the ion acoustic speed, where m_p is the proton mass. The scale length (l_n) of the expanded plasma is defined by the electron temperature (T_c), which depends on the intensity of the first pulse, and by the expansion time, t_e, or the delay between the two pulses.

Simulations with different n_p and l_n parameters were performed also with exponential density distribution on the rear side, which show significantly different results. A linear profile with a length $l_f = 3$ μm was used on the front side. The shock wave has to form close to the center in order to pass through the peak density, where the linear approximation is correct. The presented simulations were performed with the EPOCH particle-in-cell code and the results are shown in Table I. The grid size is 6.3 nm and 1000 macroparticles are used in each grid cell. The total length of the simulation box is 100 μm, where the target is placed in the middle, which ensures a large enough vacuum region for realistic acceleration. Absorbing boundaries are used for the laser fields and reflecting for the particles. The laser pulse duration is $t_L = 20$ fs in total, which starts with a 6 fs long rising edge, where the intensity increases linearly and stays constant at the peak value for the remainder of the pulse. This temporal profile was chosen to ensure a more precise comparison of simulation results with theoretical modeling, where constant intensity is considered. The effects of more realistic profiles need to be addressed in future studies. The normalized electric field amplitude is $a_0 = 20$.

For efficient heating of all electrons, the target has to be semitransparent, which requires a peak density of $n_p/n_{cr} \approx a_0/2.5$ and the sum of the density scale lengths on the rear and front sides should be around $l_n + l_f \approx ct_L = 6$ μm. These factors were chosen by considering an equivalent uniform plasma with density $n_p/2$ and length $l_f + l_n$. In a Δt time interval, the laser pulse can penetrate into the plasma $c\Delta t$ and it heats all of the incident electrons as the plasma density is relativistically under-critical. During the penetration, only 20%–30% of laser light is reflected and approximately the same amount is transmitted. The strong density perturbations eventually capture a part of the laser pulse, which results in bubble formation in higher dimensions.[28] In order to achieve nearly 100% hot electron concentration, the plasma length has to be equal to the spatial length of the laser pulse. By knowing the constraint for the plasma length, a scaling law for the hot electron temperature (T_h) can be deduced.[20] Starting from the energy balance equation: $\eta\varepsilon_L \approx \alpha T_h n_p(l_n + l_f)/2$, one can obtain

$$T_h[\mathrm{eV}] = \frac{\eta a_0^2 4.3 \times 10^{22}[\mathrm{W}]}{\alpha e n_p c}, \tag{1}$$

where η is the conversion efficiency, $\varepsilon_L = 1.37 \times 10^{22}[\mathrm{W}]$ $a_0^2 t_L/\lambda_L^2[\mu m]$ is the energy density of the laser pulse, and $\alpha = 3$ for ultra-relativistic electrons. Throughout the paper, $\lambda_L = 0.8$ μm is used for the laser wavelength.

In Table I, the properties of the energetic protons, which form a peak in the proton energy spectrum, are shown. Spectral peaks are not observable when the plasma is too dilute for the laser pulse. In the simulation corresponding to the second row, the plasma length at the front to $l_f = 4$ μm was increased in order to avoid full transparency. In plasmas with lower density (relativistically partially transparent in this case), the population of hot electrons is higher, thus the effective sound speed of ions is close to the one in one-temperature plasma:[29] $C_{s0} = \sqrt{T_h/m_p}$. In this case, the peak velocity in the shock (v_s) does not always fulfill the condition $v_s > 1.6C_{s0}$ (Refs. 30 and 17) and reflection happens rarely. The values in Table I measured in this scenario were put in

TABLE I. Parameters of simulations and proton beams. W_L is the laser energy, W_p and N_p are the energy in the peak observed in the spectrum wave and the number of protons in the peak, respectively. The total energy in the peak is $W_{p,tot}$. The values in parentheses correspond to non-reflected protons, they are in the shock wave.

t = 250 fs					
n_p/n_{cr}	l_n (μm)	W_p (MeV)	$\frac{\Delta W}{W_p}$ (%)	N_p (10^{21})	$\frac{W_{p,tot}}{W_L}$ (%)
8	2, lin.	…	…	…	…
	2, exp. ($l_f = 4$)	43	7	0.45	2.1
	5, lin.	(46)	(6.5)	(0.35)	(1.76)
	5, exp.	30	16.6	0.65	2
10	2, lin.	…	…	…	…
	2, exp.	39	12.5	0.3	1.21
	5, lin.	(18)	(22)	(3.3)	(6.18)
	5, exp.	20	40	0.77	1.68
12	2, lin.	(35)	(9.7)	(0.8)	(3)
	2, exp.	(8)	(50)	(9.2)	(8.3)
	5, lin.	(9), 15	(33), 26	(7.8), 1.45	(6.7), 2.2
	5, exp.	13	38	0.86	1.23

This article is copyrighted as indicated in the article. Reuse of AIP content is subject to the terms at: http://scitation.aip.org/termsconditions. Downloaded to IP: 129.81.226.78 On: Mon, 18 May 2015 08:13:37

parentheses, because those values are not reliable. They are changing in time, due to plasma expansion and soliton propagation.

The shock wave can remain non-reflective not only because of low peak density but also due to the linear density profile and in this case, the expansion velocity profile of the background plasma is steeper. This behavior can be seen in Fig. 1(b), which shows that the TNSA is still strong for linear density profile resulting in a linearly increasing velocity in space, similar to the standard case with sharp boundary.[11] The consequence is that the peak velocity of the solitary wave in the moving frame (in the expanding plasma) is very small. The corresponding peak in the energy spectrum is shifted towards higher energies and becomes wider, while in Fig. 1(a) the peak remains more stable. With exponential density profile, the TNSA field is much weaker[27] and the relative peak velocity of the shock wave is higher, thus the proton reflection becomes possible, which produces a well separated peak in the energy spectrum. Since the reflected protons show a much better and reliable energy distribution, this paper will only consider the exponential fall of the rear side plasma density. Using a power-law density profile, suggested in Ref. 19, with spatial dependence $(1+x/l_n)^{-\delta}$ also leads to similar results, because for any $\delta>0$, a suitable l_n to approximate the density with an exponential function can be found.

It is possible to distinguish between peaks originated from shock waves and from protons reflected by the shock wave, which usually have lower number but higher energy. This is shown in Fig. 1(a), where a deep valley separates the two parts of the spectrum, the low energy part corresponds to the background plasma (including the shock wave) and a high energy part consists of reflected protons. The high cut-off energy is a consequence of the TNSA field, which acts much stronger on the first reflected protons. Although a large energy spread is observable the energy flux of the protons in the peak is much higher than in higher energy regions of the spectrum.

According to Table I, the relativistically slightly underdense plasma is better for SWA, because of higher energy in the peak with less energy spread. If the plasma density is higher, due to the lower ion acoustic speed, proton reflection starts immediately after the formation of the shock wave. During reflection, the wave loses its energy and its peak velocity decreases, which means that the velocity of reflected protons also decreases as the shock wave propagates. This energy depletion, as well the TNSA field, causes the observed broadening of the energy spectrum, which was

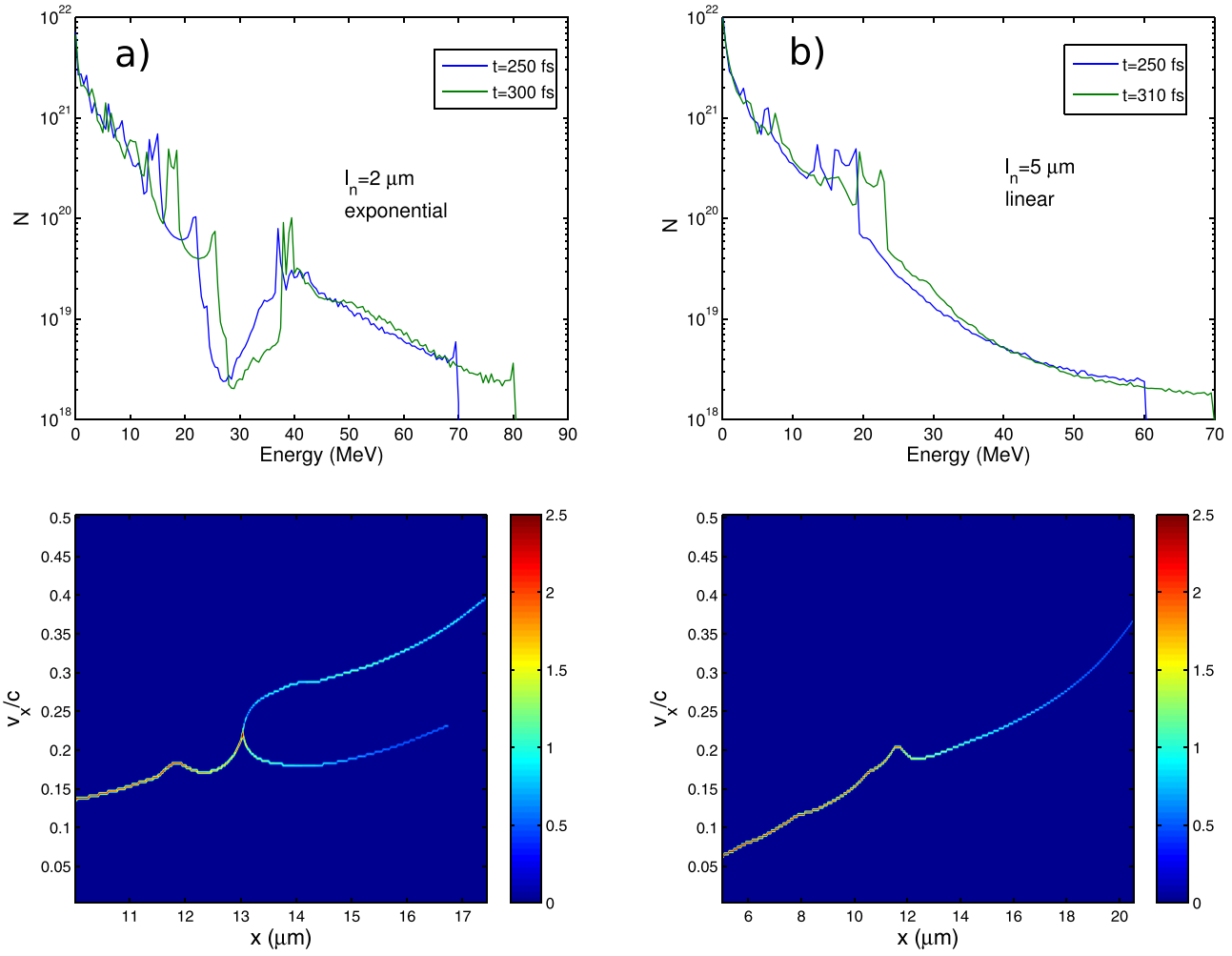

FIG. 1. Energy spectrum and corresponding velocity phase space of protons for different scale lengths and density profiles. $n_p = 10n_{cr}$. The lower pictures correspond to $t = 250$ fs.

This article is copyrighted as indicated in the article. Reuse of AIP content is subject to the terms at: http://scitation.aip.org/termsconditions. Downloaded to IP: 129.81.226.78 On: Mon, 18 May 2015 08:13:37

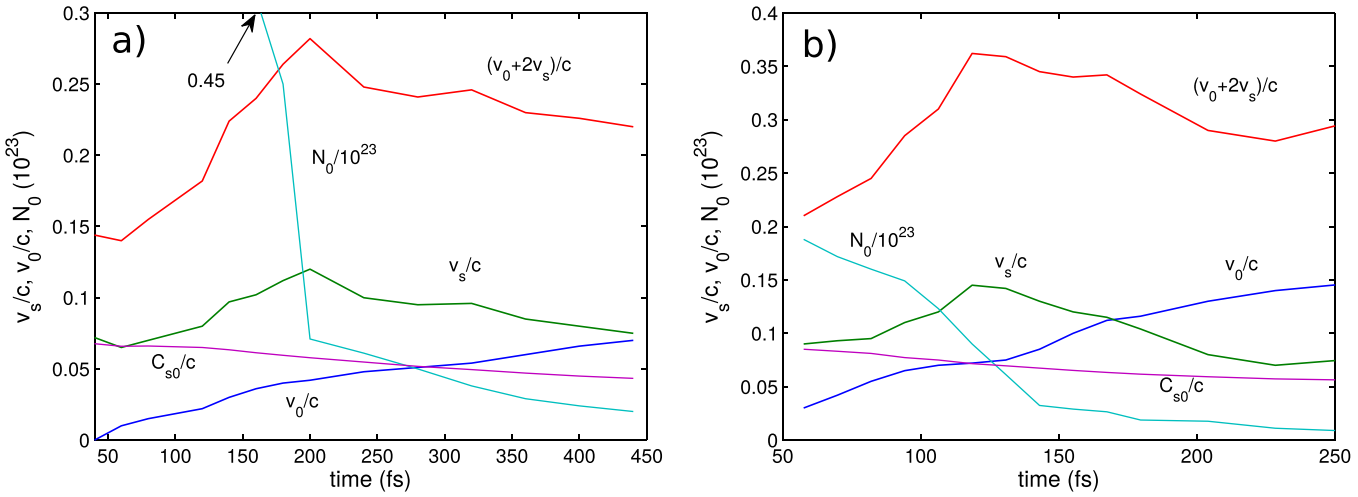

FIG. 2. Time evolution of different parameters for: $l_n = 5\ \mu$m, $l_f = 3\ \mu$m (a) and $l_n = 2\ \mu$m, $l_f = 4\ \mu$m (b). The peak density is the same $n_p = 8n_{cr}$. v_s is the peak velocity in the solitary wave, which later transforms into a shock wave (reflects protons).

noted in uniform plasma.[17] If the peak plasma density is low enough, the shock propagates in the form of a solitary wave and its peak velocity increases because of decreasing background plasma density.[24] After some time the shock wave reaches the point, where its velocity is high enough ($v_s > 1.6C_{s0}$, where v_s is the relative velocity, in the moving frame) and protons from the low density plasma get reflected. At this point, the number of protons in the background plasma is low, thus the energy depletion is slow. As the plasma expansion process has also reached its final stage, the background plasma velocity (v_0) also increases slowly and in the laboratory frame a nearly constant peak velocity of the shock wave is achieved. Consequently, the velocity spread of the reflected protons will be smaller, which is evident in Fig. 2. The protons with very similar velocities are reflected between 200–250 fs and 240–320 fs in the case of $l_n = 2\,\mu$m and $l_n = 5\,\mu$m, respectively. The corresponding peaks in the energy spectrum are shown in Fig. 3. For the shorter scale-length, the original peak is shifted to higher energy after the protons leave the plasma stream (shown at $t = 410$ fs), because of the TNSA field acting on the plasma front. For longer scale-length, the energy is lower, which is explained below.

The number of protons in the shock wave (N_0) suddenly drops in Fig. 2(a), because it splits in two parts. The second solitary wave has slightly lower peak velocity, but it will also reflect protons later, shown in Fig. 4(a). The initial areal energy density in the shock structure is about 3.9×10^9 J/m^2 and 4.4×10^9 J/m^2 for the shorter and longer scale length (with $l_f = 3\ \mu$m), respectively. The simulation was repeated with $l_f = 1\ \mu$m, where the condition for efficient heating is fulfilled. In this case, the second solitary wave is not present (see Fig. 4(b)) and the energy peak is located near the same value as in the case of shorter scale-length (Fig. 3(a)).

The decay of an initial perturbation into several separated solitons in a plasma is a well known phenomenon, which was first observed after applying a square voltages to generate the initial compression.[31,32] The compression in

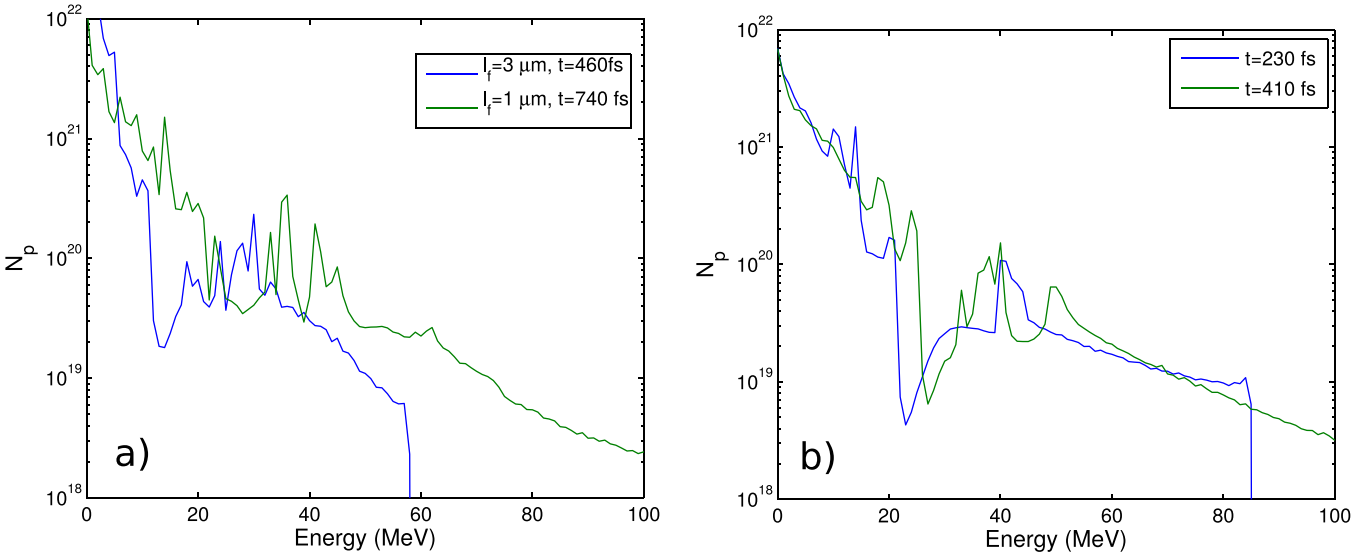

FIG. 3. Energy spectra of protons corresponding to the simulations presented in Fig. 2. The spectrum is plotted for a much later time instance in the case of $l_n = 5\ \mu$m, because the proton reflection starts later.

This article is copyrighted as indicated in the article. Reuse of AIP content is subject to the terms at: http://scitation.aip.org/termsconditions. Downloaded to IP: 129.81.226.78 On: Mon, 18 May 2015 08:13:37

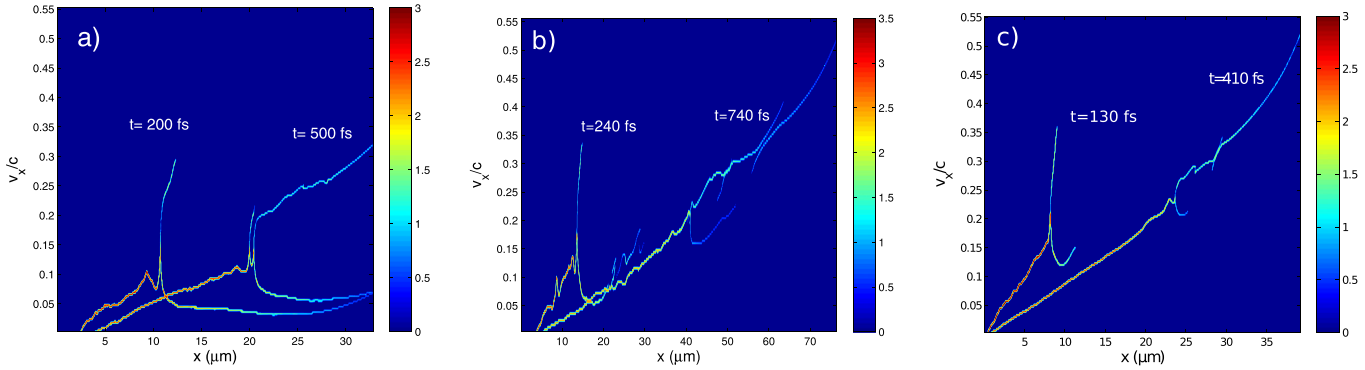

FIG. 4. Proton velocity phase space for $l_n = 5\ \mu$m, $l_f = 3\ \mu$m (a), $l_f = 1\ \mu$m (b) and $l_n = 2\ \mu$m, $l_f = 4\ \mu$m (c).

this case is done by the ponderomotive force of the laser pulse. According to the inverse scattering method, it is possible to find long-time solutions of the KdV equation, where the number of solitons is obtained by calculating the bound states of the associated Schroedinger equation.[31] In Ref. 32, the following expression is given: $(j-1)\pi = (d_s/\lambda_{De})(\delta n_0/n_0)^{1/2}$, where j is the number of solitons, d_s is the width of the compressed region of the plasma (weak shock wave), and $\delta n_0/n_0$ is the relative density growth in the shock. For the simulation presented in Fig. 4(a), $(j-1)\pi \approx 3.1$, which explains the second soliton appearing in the velocity phase-space ($j=2$). In the simulation corresponding to Figs. 4(b) and 4(c), d_s is smaller, because of shorter over-dense region of the plasma. With longer plasma length, more protons can be accelerated by the laser pulse, but they cannot propagate in the form of a single soliton. A multi-peak structure of the shock appears also with long pulses,[17] which makes the acceleration very unpredictable and the energy peak becomes broader at such high intensities.[20]

III. ANALYTICAL MODEL

In order to estimate the energy value associated with the peak in the spectrum, the initial velocity of the shock wave has to be known. This velocity gain of the protons, initially located in the vicinity of the peak density, is a consequence of the acting ponderomotive pressure of the laser pulse. The electric field produced in the target has two components: ambipolar and ponderomotive. In Ref. 33, the proton acceleration from ultra-thin and overdense foils was studied, where the relativistic transparency of the heated plasma was also included. During the laser-plasma interaction, the ponderomotive pressure is more dominant, especially in this case, where the interaction at the front side ends before the hot electrons recirculate. For the accelerating field, the following formula can be used:[33]

$$\frac{eE_{pd}}{m_e c\omega_{pe}} = \frac{1}{2\sqrt{T_h/m_e c^2}}\left[a_0/\sqrt{2}\left(1-\sqrt{1-R^2-\eta}\right)\right], \quad (2)$$

where $\omega_{pe} = (n_p e^2/m_e\epsilon_0)^{1/2}$ is the electron plasma frequency, R is the reflection, and η is the laser energy absorption coefficient. Here, $a_0 \gg 1$ was used. If a constant light pressure is assumed and the following measured values from the simulation are used, $T_h \approx 6$ MeV, $R \approx 0.3$, $\eta \approx 0.55$, the initial soliton velocity is: $v_{s0} = eE_{pd}t_L/m_i = 0.078c$, which is close to the value in Fig. 2(b). The lower energy observed in Fig. 3(a) is a consequence of the longer plasma ($l_f + l_n = 8\ \mu$m), which results in less efficient heating and thus lower C_{s0}.

Later on, as the soliton moves forward, the mass of the solitary wave will change according to the background plasma density, which will also change due to the plasma expansion. Starting from the law of energy conservation in the moving frame of the soliton, one can write

$$v_{s0}^2 = \exp[-v_s t/(l_n + v_0 t)]v_s^2. \quad (3)$$

The lower limit of l_n is on the order of the initial width of the solitary wave structure, which can be up to 1 μm wide, larger than the hot electron Debye-length, $\lambda_{De} = (T_h\epsilon_0/n_p e^2)^{1/2}$. The early stage of the propagation can be considered isothermal and the density scale length will increase with the expansion velocity, v_0. This velocity is also time-dependent and it has to be obtained from the equation of motion: $dv_0/dt = C_{s0}^2/(l_n + v_0 t)$, where the electric field $E = T_h/el_n(t)$ is uniform in the quasi-neutral region of the expanded plasma (between the peak density and the tail of the exponential profile).[27] The numerical solution can be fitted to a logarithmic function of the following form: $v_0(t) = 112C_{s0}\ln(C_{s0}t/l_n + 1)$. After evaluating v_s numerically from Eq. (3), the evolution of peak velocity, Fig. 5(a), can be obtained. The velocity starts to decrease after $\approx$1.5 time unit, which is a consequence of the isothermal assumption. The expansion of the background plasma overtakes the soliton velocity and the density at the position of the soliton starts to increase again. However, in the simulation this does not occur as the proton reflection starts earlier and the electrons cool down, thus v_0 will not increase logarithmically but reaches its maximum value asymptotically.

The time of the velocity increment, $t_i = \tau_i l_n/v_{s0}$, where τ_i is dimensionless is the most important information from Eq. (3). At this time, the shock wave reaches the maximum possible velocity: $v_{smax} \approx 1.6C_{s0}$, which is the condition for proton reflection. Fig. 5(b), plotted using a numerically computed τ_i from Eq. (3), shows that the time of velocity increment does not solely depend upon the scale-length but also on the ratio of initial ion acoustic speed and shock velocity. According to this observation, the calculated time of

This article is copyrighted as indicated in the article. Reuse of AIP content is subject to the terms at: http://scitation.aip.org/termsconditions. Downloaded to IP: 129.81.226.78 On: Mon, 18 May 2015 08:13:37

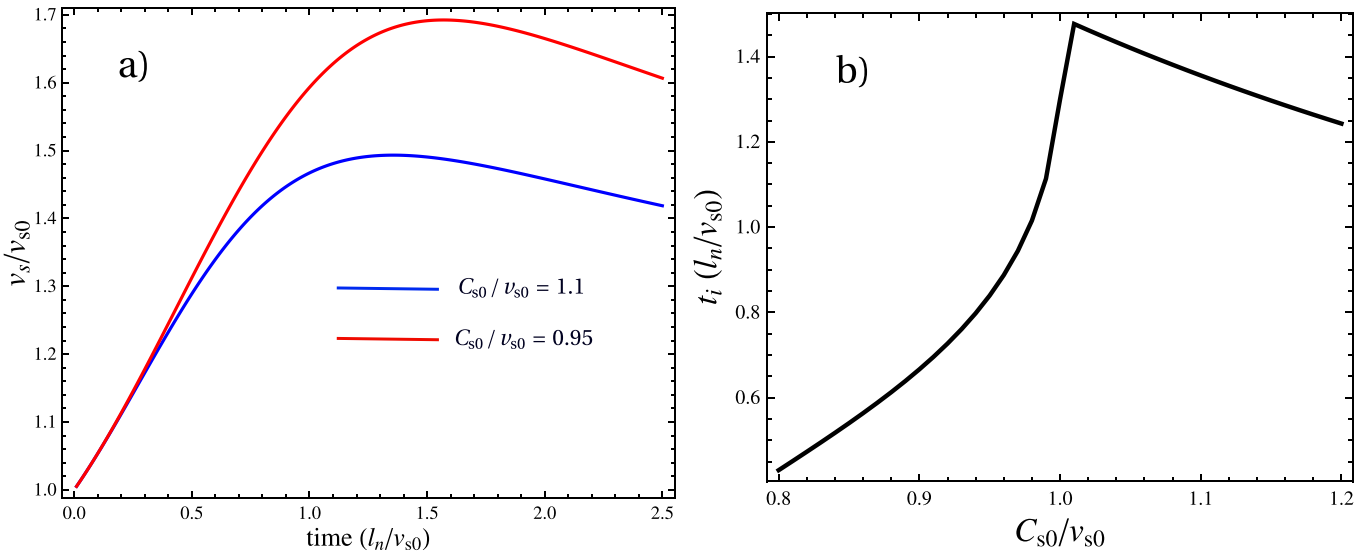

FIG. 5. Peak velocity of the soliton propagating in an exponential density profile (a), where the curves represent Eq. (3). The time needed for the soliton to reach the peak velocity equal to $1.6C_{s0}$ (b).

propagation without reflection is ≈70 fs in the case of $l_n = 2\ \mu$m and ≈170 fs for $l_n = 5\ \mu$m, which is in good agreement with the simulations presented in Fig. 2.

It can be shown that for typical parameters C_{s0}/v_{s0} varies between 0.8 and 1.2, but in the simulations it is slightly less than one. The value of τ_i, according to Fig. 5(b), varies between 0.6 and 1.4. The velocity of expanding plasma at the beginning of reflection defines the energy of the proton bunch and it can be written as $v_0(\tau_i) \approx 112C_{s0}\ln(2\pm0.4)$. The velocity of reflected protons in the laboratory frame can be stated as

$$v_{rp} = \frac{v_0(\tau_i) + 3.2C_{s0}}{1 + 3.2v_0(\tau_i)C_{s0}/c^2}. \tag{4}$$

When compared to the uniform semi-infinite plasma, protons are more energetic and the spectrum of protons shows a significant peak, which is a consequence of slow plasma expansion and slow shock depletion. In Ref. 20, v_0 has a larger contribution to the velocity of first reflected protons, whereas in this case, those protons gain more energy via reflection from the shock front. When the shock wave reaches the end of the plasma, v_0 is the dominant part in both cases. It is important to note that the acceleration mechanism in the long and short pulse regimes is nearly the same, only the density scale length has a larger impact on the final energy in the long pulse regime, which leads to a stronger scaling with laser intensity. In this study, we found that v_{rp} does not depend on l_n, a more important parameter is the ratio C_{s0}/v_{s0}, which defines the time needed for the shock wave to reach the condition for reflection.

Further simulations with higher laser intensities were also performed and compared to the analytical model derived here. For the hot electron temperature, Eq. (1) can be used, which for $n_p = n_{cr}a_0/2.5$ yields: $T_h \approx 0.24a_0$ MeV. This agrees well with the simulations, as shown in Fig. 6(a). At lower intensities, $\alpha = 3/2$ should be used, which means that the resulting electron temperature is twice as high as given by Eq. (1). Using this expression for T_h and substituting in the velocities defined earlier one yields: $v_0(\tau_i) = 1.12C_{s0}\ln(\tau_i C_{s0}/v_{s0} + 1)$, where $v_{s0} = eE_{pd}t_L$ can be calculated using Eq. (2).

In Fig. 6(b), the calculated energy $(W = (\gamma - 1)m_pc^2$, $\gamma = 1/\sqrt{1 - v_{rp}^2/c^2})$ is compared to the simulation results, where the peak density is always $n_p/n_{cr} = a_0/2.5$. The energy predicted by the model is higher than the observed values in simulations, which is due to Eq. (4) giving the velocity of the first reflected protons. The protons responsible for the peak in the energy spectrum are reflected later and they have lower velocity (see Fig. 2), because of decreasing C_{s0}. The peak in the spectrum at higher intensities is not as narrow as expected; however, the energy spread remains below 20%. The energy conversion from laser to the protons in the peak is higher than expected: 3.3% and 4.2% for $a_0 = 30$ and $a_0 = 40$, respectively.

This analysis allows a simple expression to be derived for the energy scaling (for our laser pulse duration) by knowing that $v_0 \approx (0.8\pm0.2)C_{s0}$, yielding: $W_p \sim (4C_{s0})^2/2 \sim 2a_0$ MeV, which is confirmed by Fig. 6(b).

IV. 2D SIMULATIONS

Transversal plasma instability is the strongest effect which can diminish the proton beam quality. In laser-driven proton acceleration, the Rayleigh-Taylor type of instability is the most relevant, especially in strongly over-dense plasma.[34,35] However, this type of instability is purely electrostatic, but in this case, a primarily magnetic effect, known as the Weibel instability, is present. It is always present in plasmas with anisotropic electron momentum distribution and grows exponentially in time, but its growth rate saturates for small instability wavelengths up to the value given as: $\gamma_{max} = \omega_{pe}/\sqrt{\gamma_e}$ in relativistic case.[36] For these plasma parameters, the shortest wavelength, which develops on the shortest time scale $(\gamma_{max}^{-1} \approx 4$ fs), is on the order of the hot electron Debye-length, $\lambda_{De} \approx 0.2\ \mu$m. Instabilities on larger

This article is copyrighted as indicated in the article. Reuse of AIP content is subject to the terms at: http://scitation.aip.org/termsconditions. Downloaded to IP: 129.81.226.78 On: Mon, 18 May 2015 08:13:37

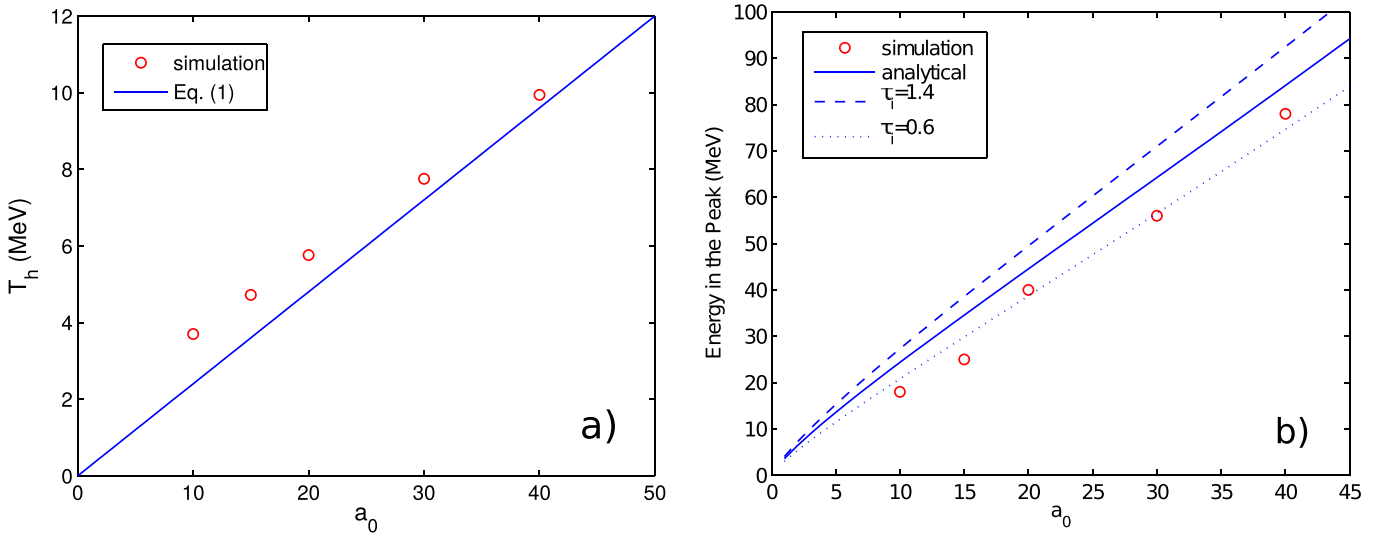

FIG. 6. Hot electron temperature compared to the analytical scaling, Eq. (1), where only fast electrons with $\gamma_e > 1.5$ are included (a). Energy of the peak in the proton spectrum (b) compared to the energy calculated from Eq. (4). In these simulations, $n_p/n_{cr} = a_0/2.5$ and $l_n = 2\,\mu$m, $l_f = 4\,\mu$m.

scales develop slower, thus they require longer pulse duration. The saturation occurs, when the growth rate becomes equal to the cyclotron frequency, which results in a magnetic field amplitude on the order of 10^5 T.

2D simulations with transversally uniform laser (planar wave) and plasma parameters have been performed to show the spatial and temporal characteristics of the Weibel instability. The width of the simulation box is 12 μm and the grid size is 12 nm in both directions. The total number of macroparticles in the simulation is 2×10^7. The plasma has the same longitudinal density profile as in the 1D simulation presented in Fig. 3(b). Transversally periodic boundaries are used. In Fig. 7(a), the proton density distribution is shown at 30 fs after the pulse reached the plasma. The short wavelength of the periodic magnetic field connected to the instability is shown in Fig. 8(a). The instability development was also tested for a 40 fs pulse where the peak density and density scale length were increased, $n_p = 10$, $l_n = 6\,\mu$m, in order to compensate for the relativistic transparency.

The filaments in the density have nearly the same amplitude for the longer pulse in Fig. 7(b), but their spatial separation is much larger, which is a consequence of the strong periodic magnetic field structure with longer wavelength, shown in Fig. 8(b). In the case of the 20 fs laser pulse, the weak filaments are smeared out by the hot electrons before reflection occurs and a uniform shock-front is formed. A stable acceleration develops with good spectral characteristics of the protons, as it is shown in Figs. 9(a) and 9(b). The regeneration of the shock front probably happens on a longer time scale in the case of 40 fs pulse, since in Fig. 9(c) the shock-wave is not well-developed and the reflection is strongly perturbed; therefore, it cannot provide narrow

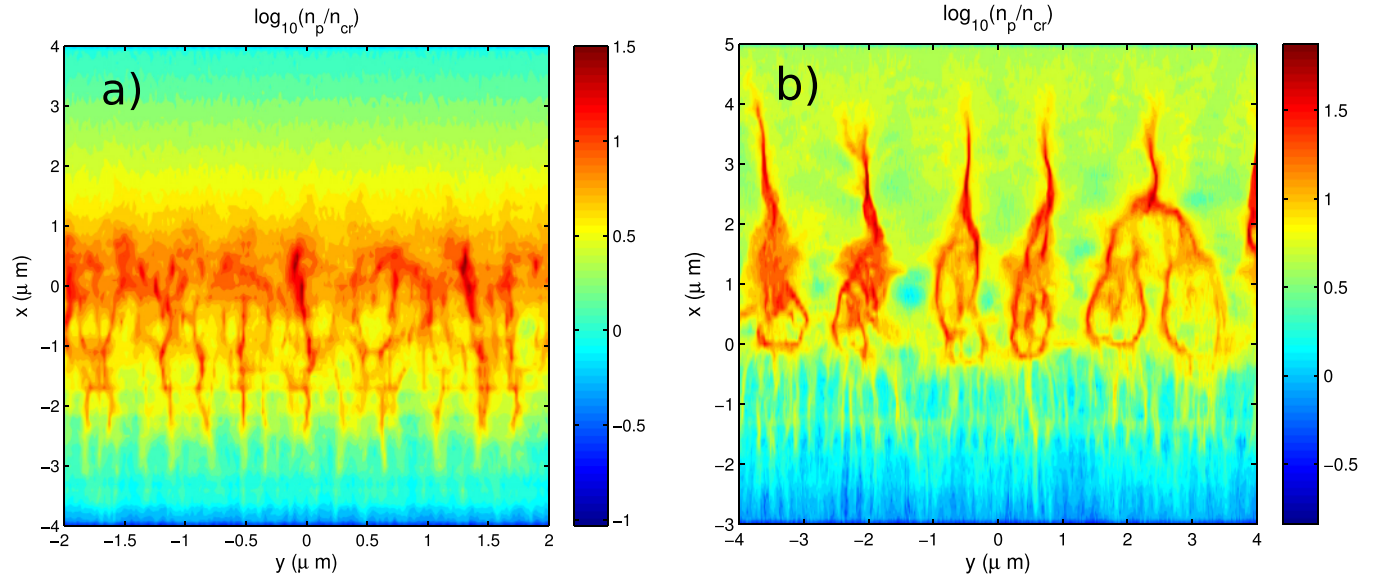

FIG. 7. Proton density distribution at 30 fs after the 20 fs long laser pulse reaches the plasma (a) and at 60 fs after the pulse with the same intensity, but with 40 fs duration, reaches the plasma (b). In the second case, the plasma density is increased to $n_p = 10 n_{cr}$ and rear density scale length to 6 μm, otherwise the simulation parameters are the same as in Fig. 3(b).

This article is copyrighted as indicated in the article. Reuse of AIP content is subject to the terms at: http://scitation.aip.org/termsconditions. Downloaded to IP: 129.81.226.78 On: Mon, 18 May 2015 08:13:37

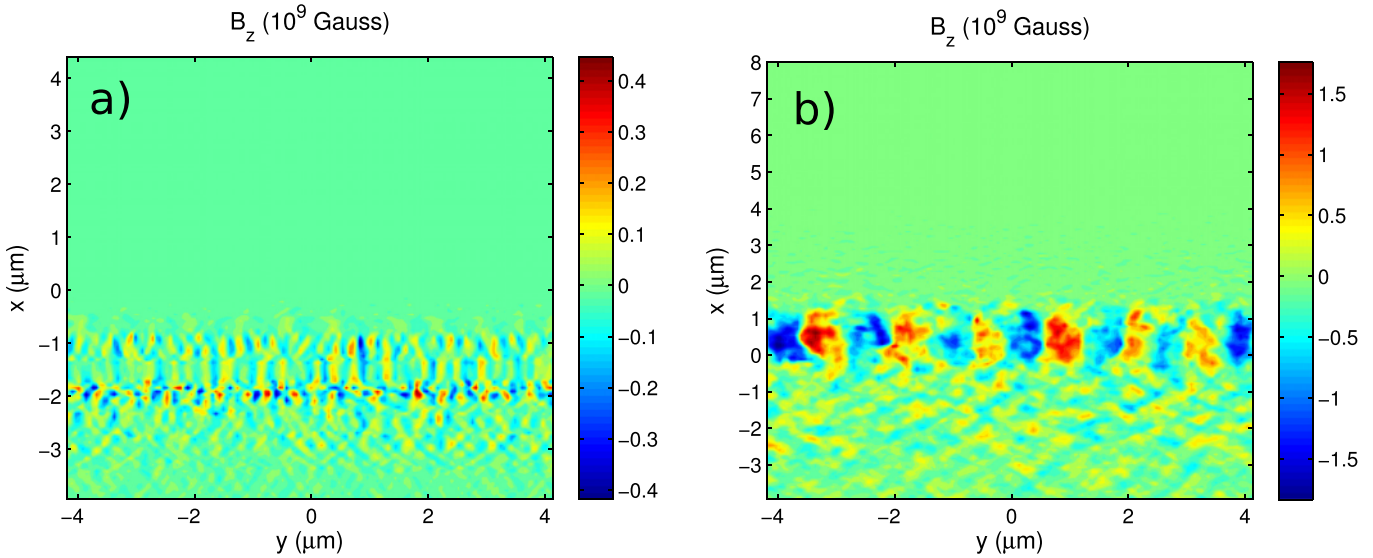

FIG. 8. The z component of the magnetic field from the simulation with 20 fs laser pulse duration at t = 15 fs (a) and with the longer pulse at t = 30 fs (b).

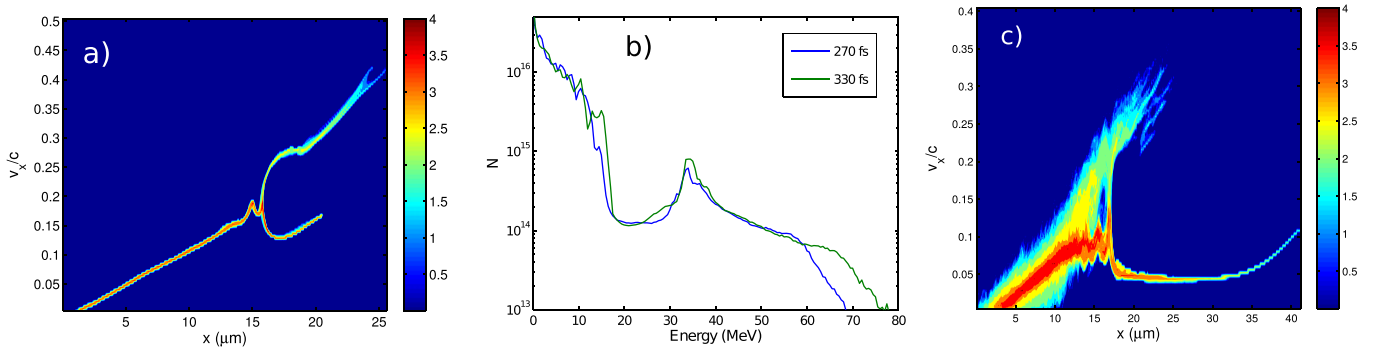

FIG. 9. Proton velocity phase-space (a) at $t = 330$ fs and corresponding energy distribution (b). The perturbed velocity phase space (c) is also shown at the same time instance for the 40 fs pulse.

energy peak. The very long density scale length used in Ref. 20 could be the reason for successful shock wave acceleration in the long pulse regime. Sentoku *et al.*[37] have shown that the maximum wavelength of instability is on the order of the laser skin depth. For higher peak density, the spatial separation of filaments is smaller. For longer pulses (>100 fs), the development of this magnetic instability depends on the laser polarization:[37] for S polarized light, the amplitude is smaller and the filaments have different structure.

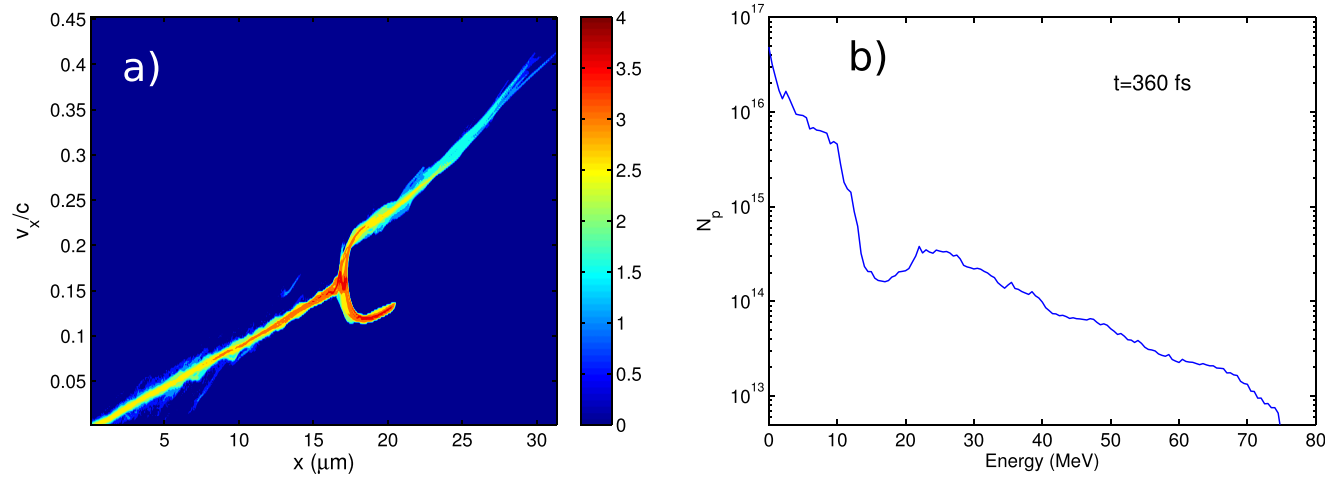

FIG. 10. Proton velocity phase-space (a) and the corresponding energy spectrum (b) of the protons between $y = -5$ μm and $y = 5$ μm. The simulation parameters are the same as in Fig. 9(a), but transversally limited flat-top laser pulse is used.

This article is copyrighted as indicated in the article. Reuse of AIP content is subject to the terms at: http://scitation.aip.org/termsconditions. Downloaded to IP: 129.81.226.78 On: Mon, 18 May 2015 08:13:37

In reality, the laser pulse has a finite focal spot size with Gaussian or flat-top transversal intensity profile. The most common Gaussian laser beam leads to very high divergence of the beam and low acceleration efficiency. One way to compensate for the non-uniformity is the shaped foil target.[34] The possibility of using wide enough laser spot with a supergauss intensity profile $\exp(-(x/w)^8)$, where $w = 10$ μm, and with 20 fs duration is explored in the next simulation. This flat-top profile is necessary to ensure strong electron heating and a stable, non-curved shock front. The width of the plasma (and simulation box) is 48 μm. The obvious effect of the finite spot size is the larger cold electron population, because electrons can enter the interaction zone laterally. The consequence is that the proton reflection starts earlier, thus the final spectrum does not contain a well-defined peak as in 1D and the peak velocity of the shock cannot increase as high as in the case of infinite laser spot size (see Fig. 10). Mass limited targets could be a solution to ensure strong heating of all electrons in the plasma.

V. CONCLUSIONS

Shock wave acceleration in expanded plasma in the short pulse regime had been described and discussed. The relevant effects of using linear or exponential density profiles had also been pointed out. While the linear density shape leads to an acceleration similar to the TNSA plasma expansion with a solitary wave moving along the downstream plasma, the exponential profile provides accelerated proton beam in a well defined, stable energy range. In order to obtain the relatively narrow energy peak in the spectrum, relativistically under-dense plasma is necessary.

The described proton acceleration is a result of the interplay between the shock-reflection and TNSA acceleration, which is weakened by the non-zero density scale-length. The energy depletion of a shock wave is an important negative effect, which has to be compensated by the slow acceleration of the background plasma, via the expansion process, and by the increasing peak velocity of the shock wave carrying less and less ions as it propagates against the density gradient. Two conditions have been found for optimal acceleration: the plasma length should be equal to the laser pulse length and the density compression by the ponderomotive pressure should not exceed $\sqrt{\delta n_0/n_0} \ll \pi\lambda_{De}/d_s$, which ensures that a single shock wave is produced.

The velocity of the reflected protons is defined by the sum of the background fluid velocity and twice the shock velocity. The energy of the peak is approximately half of the cut-off energy, but contains much more particles than the tail of the spectrum. This mechanism seems to be promising to achieve high quality proton beams, with energy scaling as $\sim 2a_0$ MeV. The analytical result in Eq. (4) is not exact, but its upper and lower limits are given. In this regime of the collisionless shock wave acceleration, the proton energy depends only on the hot electron temperature; the density scale length has an effect in the long pulse regime, which was studied in Ref. 20.

Using 2D simulations with planar laser wave results in very similar findings to the 1D geometry. Transversal instabilities can ruin the formation of the shock wave, which seems to be an issue only in the case of longer pulses. The advantage of the short pulse duration (<30 fs) is not only the single-shock production, but also the suppression of transversal instabilities. With finite laser spot size, smaller peak in the spectrum at lower energy is observed due to the transversal degree of freedom of electrons. Size limited targets or larger laser spot size could be more effective.

[1]T. E. Cowan, J. Fuchs, H. Ruhl, A. Kemp, P. Audebert, M. Roth, R. Stephens, I. Barton, A. Blazevic, E. Brambrink *et al.*, Phys. Rev. Lett. **92**, 204801 (2004).
[2]L. Romagnani, J. Fuchs, M. Borghesi, P. Antici, P. Audebert, F. Ceccherini, T. Cowan, T. Grismayer, S. Kar, A. Macchi *et al.*, Phys. Rev. Lett. **95**, 195001 (2005).
[3]M. Nishiuchi, H. Daido, A. Sagisaka, K. Ogura, S. Orimo, M. Kado, A. Yogo, M. Mori, Y. Hayashi, S. Bulanov *et al.*, Appl. Phys. B **87**, 615 (2007).
[4]I. Hofmann, J. Meyer-ter-Vehn, X. Yan, A. Orzhekhovskaya, and S. Yaramyshev, Phys. Rev. ST Accel. Beams **14**, 031304 (2011).
[5]U. Linz and J. Alonso, Phys. Rev. ST Accel. Beams **10**, 094801 (2007).
[6]H. Daido, M. Nishiuchi, and A. S. Pirozhkov, Rep. Prog. Phys. **75**, 056401 (2012).
[7]S. C. Wilks, A. B. Langdon, T. E. Cowan, M. Roth, M. Singh, S. Hatchett, M. H. Key, D. Pennington, A. MacKinnon, and R. A. Snavely, Phys. Plasmas **8**, 542 (2001).
[8]Z. Lecz, O. Boine-Frankenheim, and V. Kornilov, Nucl. Instrum. Methods Phys. Res., Sect. A **727**, 51 (2013).
[9]M. Passoni and M. Lontano, Phys. Rev. Lett. **101**, 115001 (2008).
[10]B. M. Hegelich, B. J. Albright, J. Cobble, K. Flippo, S. Letzring, M. Paffett, H. Ruhl, J. Schreiber, R. K. Schulze, and J. C. Fernandez, Nature **439**, 441 (2006).
[11]P. Mora, Phys. Rev. Lett. **90**, 185002 (2003).
[12]J. Fuchs, P. Antici, E. d'Humiéres, E. Lefebvre, M. Borghesi, E. Brambrink, C. A. Cecchetti, M. Kaluza, V. Malka, M. Manclossi *et al.*, Nat. Phys. **2**, 48–54 (2006).
[13]T. Zh. Esirkepov, M. Borghesi, S. V. Bulanov, G. Mourou, and T. Tajima, Phys. Rev. Lett. **92**, 175003 (2004).
[14]B. Qiao, M. Zepf, M. Borghesi, B. Dromey, M. Geissler, A. Karmakar, and P. Gibbon, Phys. Rev. Lett. **105**, 155002 (2010).
[15]T. Schlegel, N. Naumova, V. T. Tikhonchuk, C. Labaune, I. V. Sokolov, and G. Mourou, Phys. Plasmas **16**, 083103 (2009).
[16]A. Macchi, S. Veghini, and F. Pegoraro, Phys. Rev. Lett. **103**, 085003 (2009).
[17]A. Macchi, A. S. Nindrayog, and F. Pegoraro, Phys. Rev. E **85**, 046402 (2012).
[18]L. O. Silva, M. Marti, J. R. Davies, R. A. Fonsesca, C. Ren, F. S. Tsung, and W. B. Mori, Phys. Rev. Lett. **92**, 015002 (2004).
[19]A. A. Andreev, A. G. Zhidkov, A. Sasaki, and K. Yu. Platonov, Plasma Phys. Controlled Fusion **44**, 1243 (2002).
[20]F. Fiuza, A. Stockem, E. Boella, R. A. Fonseca, L. O. Silva, D. Haberberger, S. Tochitsky, W. B. Mori, and C. Joshi, Phys. Plasmas **20**, 056304 (2013); F. Fiuza, A. Stockem, E. Boella, R. A. Fonseca, L. O. Silva, D. Haberberger, S. Tochitsky, C. Gong, W. B. Mori, and C. Joshi, Phys. Rev. Lett. **109**, 215001 (2012).
[21]D. Haberberger, S. Tochitsky, F. Fiuza, C. Gong, R. A. Fonseca, L. O. Silva, W. B. Mori, and C. Joshi, Nat. Phys. **8**, 95 (2012).
[22]C. A. J. Palmer, N. P. Dover, I. Pogorelsky, M. Babzien, G. I. Dudnikova, M. Ispiriyan, M. N. Polyanskiy, J. Schreiber, P. Shkolnikov, and V. Yakimenko, Phys. Rev. Lett. **106**, 014801 (2011).
[23]P. Antici, J. Fuchs, E. d'Humieres, J. Robiche, E. Brambrink, S. Atzeni, A. Schiavi, Y. Sentoku, P. Audebert, and H. Pepin, New J. Phys. **11**, 023038 (2009).
[24]A. Zhidkov, M. Uesaka, A. Sasaki, and H. Daido, Phys. Rev. Lett. **89**, 215002 (2002).
[25]M. Gauthier, A. Lévy, E. d'Humieres, M. Glesser, B. Albertazzi, C. Beaucourt, J. Breil, S. N. Chen, V. Dervieux *et al.*, Phys. Plasmas **21**, 013102 (2014).
[26]A. V. Gurevich, L. V. Pariiskaya, and L. P. Pitaevskii, Sov. Phys. JETP **22**, 449 (1966).
[27]T. Grismayer and P. Mora, Phys. Plasmas **13**, 032103 (2006).

This article is copyrighted as indicated in the article. Reuse of AIP content is subject to the terms at: http://scitation.aip.org/termsconditions. Downloaded to IP: 129.81.226.78 On: Mon, 18 May 2015 08:13:37

[28]S. C. Wilks, W. L. Kruer, M. Tabak, and A. B. Langdon, Phys. Rev. Lett. **69**, 1383 (1992).
[29]A. Diaw and P. Mora, Phys. Rev. E **84**, 036402 (2011).
[30]J. Denavit, Phys. Rev. Lett. **69**, 3052 (1992).
[31]M. Q. Tran, Phys. Scr. **20**, 317 (1979).
[32]N. Hershkowitz, T. Romesser, and D. Montgomery, Phys. Rev. Lett. **29**, 1586 (1972).
[33]A. Andreev, K. Yu. Platonov, M. Schnuerer, R. Prasad, and S. Ter-Avetisyan, Phys. Plasmas **20**, 033110 (2013).
[34]T. Pu-Yu, A. Pukhov, G. Shvets, and M. Chen, Phys. Rev. Lett. **105**, 065002 (2010).
[35]F. Pegoraro and S. V. Bulanov, Phys. Rev. Lett. **99**, 065002 (2007).
[36]P. H. Yoon and R. C. Davidson, Phys. Rev. A **35**, 2718 (1987).
[37]Y. Sentoku, K. Mima, S. Kojima, and H. Ruhl, Phys. Plasmas **7**, 689 (2000).

This article is copyrighted as indicated in the article. Reuse of AIP content is subject to the terms at: http://scitation.aip.org/termsconditions. Downloaded to IP: 129.81.226.78 On: Mon, 18 May 2015 08:13:37